Study of the ITER TF CICC Mechanical Behavior Under Cool-Down and Repetitive EM Loadings

Rebecca Riccioli, Alexandre Torre, Damien Durville, Marco Breschi, Frederic Lebon, Vladimir Tronza

Study of the ITER TF CICC Mechanical Behavior Under Cool-Down and Repetitive EM Loadings

Rebecca Riccioli, Alexandre Torre, Damien Durville, Marco Breschi, Frederic Lebon, and Vladimir Tronza

High-current and high-field superconducting mag-nets sustain huge electromagnetic loads. On top of that, the high field constraint pushes towards the use of high-performing super-conducting Nb_3Sn strands, which are strain sensitive. In recent fusion magnets, the loads reach few hundreds of kN/m in static and sometimes cyclic regimes. These loads modify the strands local strain state and the overall mechanical properties of the cable. In this article, the finite element mechanical code MULTIFIL is applied to model an ITER Cable-In-Conduit Conductor (CICC) petal for the Toroidal Field (TF) coil under operating loadings. The local strain maps and the macroscopic mechanical behavior of the cable are analyzed for both thermal and electromagnetic loadings. A possible explanation for the initial drop of the current sharing temperature observed in some of the TF CICCs tested in the SULTAN facility (PSI, Villigen) is proposed. The impact of important model parameters, such as the void fraction and the friction coefficient between strands, on the mechanical behavior of the conductor is investigated.

Keywords—Superconductors, Nb_3Sn, Strain-sensitiveness, Fusion Magnets, Cable-In-Conduit Conductors.

I. Introduction

The strands of the Cable-In-Conduit Conductors (CI-CCs) for the International Thermonuclear Experimental Reactor (ITER) magnet system Toroidal Field (TF) coils are composite wires containing filaments of Nb3Sn. These strands exhibit a critical current density that strongly depends on the strain state of the superconducting filaments [1]. During the operation, the conductors are submitted to a thousand electro-magnetic (EM) cycles and a hundred thermal cycles [2] affecting the Nb3Sn mechanical state, as also the cable current carrying capability.

Rebecca Riccioli is with CEA, Commissariat à l'énergie atomique et aux énergies alternatives, Cadarache, 13115 Saint-Paul-Lez-Durance, France, with the Aix-Marseille Université, 13013 Marseille, France, and also with the Bologna University, 40136 Bologna, Italy (e-mail: rebecca.riccioli@cea.fr).

Alexandre Torre is with CEA, Commissariat à l'énergie atomique et aux énergies alternatives, Cadarache, 13115 Saint-Paul-lez-Durance, France.

Damien Durville is with MSSMat Laboratory (Mechanics of Soils, Structures and Materials), Centrale Supélec, CNRS UMR8579, Université Paris Saclay, 91190 Gif-sur-Yvette, France.

Marco Breschi is with the Department of Electrical, Electronic and Information Engineering, University of Bologna, 40136 Bologna, Italy.

Frederic Lebon is with the Aix-Marseille Université, CNRS, Centrale Marseille, LMA (Laboratoire de Mécanique et Acoustique) 13013 Marseille, France.

Vladimir Tronza is with IO (ITER Organization) 13115 Saint-Paul-Lez-Durance, France.

The work of this article is based on an upgraded version of the electromechanical model of the ITER TF CICC. This model was implemented in the MULTIFIL code, which solves the mechanical equilibrium of bundles made of hundreds of multi-twisted strands [3]–[5]. The main goal is to investigate the macroscopic mechanical behavior of the simulated conductor during the cool-down and the first EM cycles. This analysis allows one to make preliminary hypotheses on the evolution of the current sharing temperature (T_{cs}) with EM cycles [6], with special reference to the measured initial drop. Two parametric studies were conducted to analyze the dependence of the cable mechanical behavior on important parameters (friction coeffi-cient and void fraction). A focus is made on the evolution of contacts between strands and on fractures as a function of these parameters.

II. The Mechanical Simulations

A. The Simulations With MULTIFIL Code

MULTIFIL is a finite element simulation code that provides the local strain map at the level of the strands of the cable [7]. As exhaustively explained in a previous work [4], the loading sequence for the simulation of the CICC starts from the manufacturing of the cable, followed by the heat treatment (HT) at 650 °C and by the application of the thermal and EM loadings.

The thermal loadings exert a longitudinal stress on the Nb_3Sn filaments [8] and are simulated by imposing an axial displacement to one end of the petal. This applied strain ε_{ap} is an input data since the jacket is just geometrically represented in MULTIFIL. A method is presented in [5] to compute the mechanical equilibrium between the stainless steel jacket, with known mechanical properties, and the simulated cable.

For the EM loadings, each superconducting strand is subjected to a linear load of 0.89 kN/m (11.78 T, 68 kA). An additional load is simultaneously applied to the petal through the boundary conditions, which allows accounting for the cumulative effect of the other petals on the simulated one [5].

B. Definition of the Cable Mechanical Parameters

In MULTIFIL the strands are described by elastoplastic laws at room temperature (RT) [9]. The strain is calculated at 9 points on the strand cross-sectional surface and for each node the axial strain ε_{ax} and the bending strain ε_b are found [4]. Recently,

TABLE I
ITER TF CIC CONDUCTOR PARAMETERS

Cabling layout	((2sc+1Cu)x3x5x5 +(3x4Cu))x6
Central spiral	8x10 mm
Petal wrap	0.10 mm thick, 50 % cover
Cable wrap	0.10 mm thick, 40 % overlap
Cr coated strand diameter	0.82 mm
Strands number	1422
Void Fraction (annulus)	29.7 %
Cable diameter	39.7 mm
SS 316LN jacket outer diameter	43.7 mm

the outputs of the code were redefined to discriminate, at each calculation node and for each point of the cross-section, the elastic ε^{el} and plastic ε^{pl} components of the local strain.

Mechanical parameters, extracted from the MULTIFIL results, are defined to help understanding the mechanical status of the cable at various loading steps and to compare the different analyzed cables. First, the plasticity ratio η^{pl} defined as:

$$\eta^{pl} = \left|\langle\varepsilon^{pl}_{ax}\rangle / \langle\varepsilon^{el}_{ax}\rangle\right|$$

where $\langle\varepsilon^{el}_{ax}\rangle$ is the elastic contribution to the average strain on the axis of the strands and $\langle\varepsilon^{pl}_{ax}\rangle$ is the plastic one, i.e., $\langle\varepsilon_{ax}\rangle = \langle\varepsilon^{pl}_{ax}\rangle + \langle\varepsilon^{el}_{ax}\rangle$. η^{pl} allows one to study the level of plasticization of the cable. Second, the bending ratio γ^b, given by

$$\gamma^b = \left|\langle\varepsilon_b\rangle / \langle\varepsilon_{ax}\rangle\right|$$

indicates weather the cable behaves more as a rigid bundle ($\gamma^b < 1$) or as a helical spring ($\gamma^b > 1$). In the first case, any applied strain is converted mainly into axial strain, while in the second one into bending. Third, the cable axial strain transfer coefficient ${\alpha_{ax}}^t$ is calculated as the variation of the average axial strain $\langle\varepsilon_{ax}\rangle$ divided by the applied strain ε_{ap} during the same range. It defines the percentage of the applied longitudinal strain transferred to the strands as axial strain.

In the following sections we will also refer to the longitudinal reaction force F_z, which corresponds to the resultant force applied along the axis of the analyzed petal at its extremities, scaled to a full cable. In order to obtain macroscopic properties of the cable, the stress σ_z is calculated as F_z/S_{cable}, where S_{cable} is the cross-sectional surface of the annular part of the cable, used to have a homogenized behavior.

Finally the Young's modulus E_0 is calculated via the method presented for the tensile tests in [10], adapted here to the compressive stress $\sigma_{z,strands}$. The latter is defined as $F_z/S_{strands}$, where $S_{strands}$ is the cross-sectional surface of the strands ${N_s}{r_s}^2\pi$. E_0 corresponds to the initial slope of the linear part of the unloading curve at -0.2% of applied compressive strain [10].

III. NOMINAL CASE STUDY

The current model of the ITER TF CICC is based on the design parameters reported in Table I [11]. To limit the computation time, only a length of 300 mm of the last cabling stage of the cable (called *petal*) is simulated. The petal axis is assumed rectilinear, thus neglecting the twist of the last cabling stage. The TF CICC petals are wrapped with stainless steel for mechanical reinforcement; differently from other works [4]–[5], the wrappings contribution to the total void fraction is considered. The mean twist angle calculated with the MULTIFIL code is 0.987,

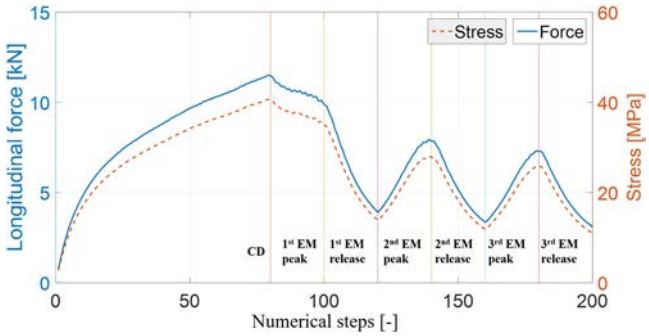

Fig. 1. Longitudinal reaction force F_z and stress σ_z of the cable for the given sequence of loadings applied to the nominal case study.

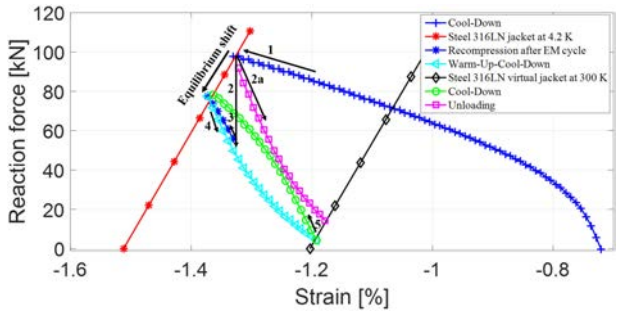

Fig. 2. Study of the mechanical equilibrium between the virtual stainless steel jacket (in red at 4.2 K and in black at 300 K) and the simulated cable after the different loadings for different temepratures. The abscissa is the relative strain with respect to the 923.15 K.

which is greater than the design value of 0.97 because of the absence of the last cabling stage.

The effect on F_z and σ_z of the loadings applied are presented in Fig.1 and discussed in the following sections.

A. The Cool-Down Simulation

As mentioned in section II.A, for the simulation of the cool-down (CD) from 923.15 K to 4.5 K, it is necessary to know the global compressive strain applied to the petal [5]. An applied strain of -0.61% is found for the baseline study.

For the CD, the (ε, σ_z) mechanical characteristics was fitted by means of a fitting function where the linear part [9] represent the elastic behavior of the Nb_3Sn [12]. The goal is to provide the mechanical properties of the homogenized cable to perform studies where the macroscopic behavior of the cable are required without simulating it. The fitting function for σ_z includes three parameters (α, β, γ):

$$\sigma_z = \alpha\left(1 - e^{-\beta\varepsilon}\right) + \gamma\varepsilon$$

As shown in Fig. 2, after the CD, different possible loading sequences are investigated. In a first sequence, a simple warm-up (WU) (2a) is applied until the mechanical equilibrium between cable and jacket at 300 K is reached. A second sequence consists of an EM cycle (2), followed by a recompression of the cable (3) and a warm-up-cool-down (WU-CD) (4 and 5) at 300 K. The abscissa of Fig. 2 is the relative strain with respect to the thermal treatment temperature (923.15 K) [5]. The main results obtained for each loading are reported in Table II, where ε_{ax} and ε_{pl} refer to the average values, and discussed in section II.E.

TABLE II
STRAIN BEHAVIOR OF THE NOMINAL CASE FOR DIFFERENT LOADINGS

Loadings	ε_{ap} [%]	ε_{ax} [%]	γ^{p} [-]	ε_{pl} [%]	η^{pl} [-]
Cool Down	–0.610	–0.451	0.539	–0.322	2.5
1 EM + RC	–0.0422	–0.476	0.561	–0.440	12.3
Warm Up	+0.152	–0.342	0.580	–0.354	29.7
[Warm Up	[+0.177	[–0.365	[0.557	[–0.421	[7.5
- Cool Down]	–0.169]	–0.469]	0.562]	–0.432]	11.7]
3 EM + RC	–0.0254	–0.487	0.594	–0.476	46.3

B. The First EM Cycle Simulation

After the first CD, an EM cycle was applied by following the method introduced in section II.A [5]. Fig. 1 shows that the longitudinal reaction force of the cable decreases during the application of the Lorentz force. Even though the average axial strain is almost constant at -0.45% for the CD and after the first EM cycle, the plasticity ratio instead dramatically changes from 2.5 to 13.7. These results suggest that the major effect of the first EM cycle is the plasticization of the cable. Since the longitudinal reaction force significantly decreases, it is reasonable to expect that a new equilibrium between the jacket and the cable is established. To reach the new equilibrium, a recompression of the cable of -0.042% is required with respect to the equilibrium found at the end of the CD and in Table II the results are reported considering the EM cycle and its recompression as well.

C. The Warm-Up-Cool-Down and the Warm-Up

The impact on the cable behavior of the aforementioned loading sequences was also investigated. The effect of a WUCD cycle between cryogenic and RT after the first EM cycle was studied and a WU to RT was simulated directly after the CD as well. In both cases, a new cable-jacket equilibrium is established at RT [5]. The main results are reported in Table II. Differently from real cable, the simulation of the WUCD does not show a major impact on the local strain maps, and does not permit a better understanding of the WUCD degradation for now.

D. Impact of Several EM Cycles

After the first EM cycle, the simulation continues with the application of three further EM cycles. A recompression to keep the cable-jacket equilibrium should be applied after each EM cycle. For simplicity, only one recompression of -0.0254% is applied here at the end of the 3 EM cycles. The simulation results are exposed in Table II and discussed in section III.E.

E. Discussion and Preliminary Explanations

The results reported in Table II show that the cable is only slightly plasticized after the first CD, while both the WU and the first EM cycle result in a significant plasticization of the cable, as indicated by the η^{pl} value. When the cable plasticizes, the jacket relaxes and tends to its rest point as if it were free. The initial calculated strain after CD is $+0.18\%$ for the jacket and -0.61% for the cable with respect to their rest positions at 4.2 K. This means that after CD the jacket has a "reserve" compressive strain of -0.18% that it applies to the cable during the EM cycling because of the cable's softening. The calculation shows that after $\sim$100 EM cycles, the rest point of the jacket is reached. The progressive plasticization of the cable and corresponding relaxation of the jacket could explain the initial drop of the T_{cs} observed in several TF conductors [6]. The cable axial strain transfer coefficient ${\alpha_{ax}}^{t}$ after the 1st EM cycle recompression is 0.64 and it is calculated as the $\Delta\varepsilon_{ax}$ between the EM cycle and its recompression divided by the ε_{ap} during the recompression. Multiplying ${\alpha_{ax}}^{t}$ by the reserve compressive strain of the jacket, the obtained value is added, as a first approximation, to the effective strain retrieved from measurements [13]. Adding this further strain produces a T_{cs} drop of around 0.6 K, calculated with the critical surface parametrization of the left leg of the SULTAN sample TFEU12 [6]. The ΔT_{cs} is within the experimental results range ($0.2-0.7$ K) of the tested TF conductors drops [6], [14].

TABLE III
MECHANICAL BEHAVIOR FOR FIVE VFS AFTER CD

	27.8 %	**29.7 %**	32.7 %	35.3 %	36 %
α [MPa]	128.67	**140.18**	139.39	131.03	115.61
β [MPa]	13.44	**15.75**	11.95	10.0501	10.00
γ [MPa]	587.31	**363.73**	156.93	54.28	50.31
E_0 [GPa]	109	**105**	86.9	73.2	70.7
ε_{ap} [%]	–0.56	**–0.61**	–0.67	–0.7	–0.7
ε_{ax} [%]	–0.49	**–0.45**	–0.31	–0.21	–0.19
γ^{p} [-]	0.30	**0.54**	1.09	1.68	1.82
ε_{pl} [%]	–0.37	**–0.32**	–0.21	–0.14	–0.12
η^{pl} [-]	2.9	**2.5**	2.0	1.8	1.7

TABLE IV
MECHANICAL BEHAVIOR FOR FIVE VFS AFTER ONE EM CYCLE

	27.8 %	**29.7 %**	32.7 %	35.3 %	36 %
ε_{ap} [%]	–0.025	**–0.042**	–0.051	–0.042	–0.51
ε_{ax} [%]	–0.51	**–0.48**	–0.32	–0.21	–0.20
γ^{p} [-]	0.33	**0.56**	1.16	1.85	1.98
ε_{pl} [%]	–0.44	**–0.44**	–0.33	–0.22	–0.20
η^{pl} [-]	6.3	**12.3**	52	103	67

TABLE V
MECHANICAL BEHAVIOR FOR SEVERAL FRICTIONS AFTER CD

	0.1	0.2	0.5	0.7	0.9
E_0 [GPa]	**105**	109	115	116	116
ε_{ap} [%]	**–0.61**	–0.6	–0.59	–0.58	–0.57
ε_{ax} [%]	**–0.45**	–0.464	–0.473	–0.472	–0.472
γ^{p} [-]	**0.54**	0.473	0.395	0.371	0.348
ε_{pl} [%]	**–0.32**	–0.334	–0.344	–0.348	–0.352
η^{pl} [-]	**2.5**	2.6	2.7	2.8	2.9

IV. PARAMETRIC STUDIES

The main purpose of this section is to discuss the impact of the void fraction and of the friction coefficient between strands on the mechanical behavior of the cable. The nominal case study is characterized by a VF of 29.7% and a friction coefficient between strands of 0.1. Four further case studies were investigated with a VF of 27.8%, 32.7%, 35.3% and 36% respectively. For all of them, a sequence of CD and one EM cycle with its recompression was applied. The summary of the mechanical results describing the computed strain distributions are presented in Table III for the CD and Table IV for the EM cycle. The CD was analyzed in function of different friction coefficients ranging from 0.1 to 0.9 and Table V reports results obtained for the friction coefficients 0.1, 0.2, 0.5, 0.7 and 0.9.

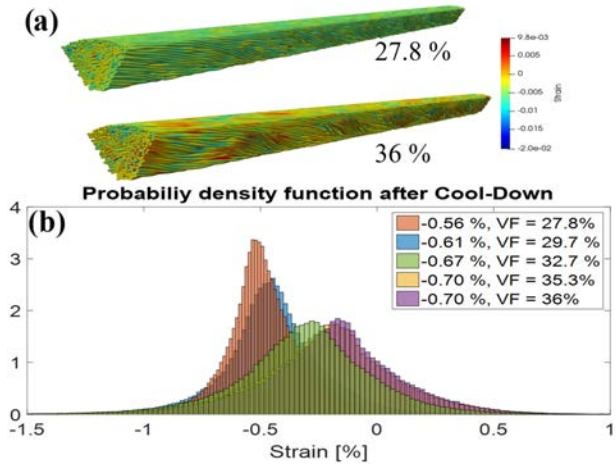

Fig. 3. (a) MULTIFIL strain map after CD for two different VFs. (b) Strain distribution after CD as a function of the VF.

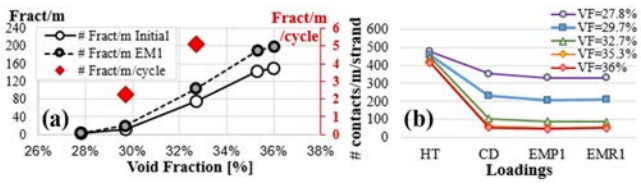

Fig. 4. (a) For each loading, variation of the number of fractures per meter as a function of the VFs. (b) For each loading, variation of the contacts number per meter and per strand as a function of the VFs.

A. Discussion on the Macroscopic Mechanical Results

As expected, E_0 increases with increasing the friction coefficient and decreasing the VF. The same behavior is shown by the applied strain ε_{ap} during the CD to achieve the thermal equilibrium with the jacket at 4.5 K. As for the plasticity, the coefficient η^{pl} clearly indicates that it increases with the friction coefficient and decreases with the VF. The CD affects more the η^{pl} of the less compacted cables that will be less subjected to the major plasticization due to the EM cycles. The γ^b values indicate that the bending phenomenon is predominant for the softer cables with lower strand friction coefficients and higher VFs, as also confirmed by the strong buckling observed in Fig.3a). Tables III and IV show an inversion of the tendency of γ^b between 29.7% and 32.7%, thus highlighting a change of the cable behavior that can be related to the transition between the locked and the loose regimes identified in [15]. Fig. 3b) shows the same behavior in terms of the strain distribution. The distribution clearly switches from strict and peaked to be larger and flatter for greater void fractions. In this study the nominal case is a locked cable; in real conductors we expect to find this threshold at a lower VF since for the given twist pitches ($cos\vartheta$ of 0.97), a VF of 29.7% should correspond to a loose cable [15]. It is however interesting to observe its qualitative detection and reproduction with the code.

B. Fractures and Contacts Study

Fig. 4a) reports the number of fractures per meter of conductor occurring at tensile strain with a filament breakage level set to $+0.2\%$ [16]. The counted fractures are studied after each loading

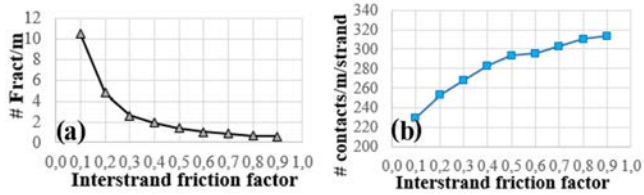

Fig. 5. (a) Variation of the number of fractures per meter as a function of friction after CD. (b) Variation of the contacts number per meter and strand as a function of friction factor after CD.

and increase with the VF, highlighting the transition from locked to loose behavior. The impact of the EM cycles on the fractures increases with the VF as illustrated by the number of fractures per meter per cycle for two different VFs. At the same time the EM cycles show a start of the fatigue phenomenon. The analysis performed at the end of the CD (Fig. 5a)) confirms that as the friction coefficients increases, the fractures per meter decrease, and a threshold around 0.2–0.3 is observed.

The study of contacts [17] is important for the analysis of the AC losses, since they should affect the interstrand resistances [18]. The plots in Fig. 4b) and Fig. 5b) report the number of contacts, which are the same as after the heat treatment simulation. This study is focused on the contacts created during the manufacturing of the cable, which will be characterized by low resistance [17] and it aims to study how they evolve during the mechanical loadings. The plots refer to the number of contacts per meter and strand. Fig. 5a) shows that the most compacted cables are characterized by stronger contacts after the manufacturing phase. It was observed also that the average normal contact force is greater for the lower VFs; the effect of the Lorentz force is to add an extra-force that is significantly greater for the highest values of the VF. Considering that the interstrand conductances increase with decreasing the VF [19] and that it was experimentally observed an increase of the $n\tau$ value of 3 times from 36% to 26% of the VF [20], all the observations about the contacts are in accordance with AC losses evolution as a function of the compaction ratio.

The Fig. 5b) refers to the contacts after CD, and shows that higher friction coefficients make the cable preserve the strong contacts created during manufacturing.

V. Conclusion

The study of the baseline ITER TF conductor configuration suggests that the cable plasticization occurring with the first EM cycles produces a jacket relaxation and, correspondingly, a softening and further compression of the cable. This physical mechanism might explain the initial T_{cs} drop found experimentally on many ITER TF conductors [6]. The simulated WUCD does not seem to affect the cable behavior, but it would be interesting to investigate its impact on a loose configuration.

The performed parametric studies show a clear transition from the locked to the loose behavior through the evolution of fractures, contacts and bending ratio. The code indicates very different behaviors of the cable as a function of its compaction ratio and as expected by [15], [20].

Further studies will be performed by applying additional cyclic loadings, to quantitatively assess the T_{cs} drop, also through the coupling with detailed electromagnetic models.

Finally, other modelling assumptions will be removed, like the rectilinear configuration of the petal, to get a more accurate placement of the transition from the locked to the loose cable properties.

References

[1] D. Ciazynski, "Review of Nb_3Sn conductors for ITER," *Fusion Eng. Des.*, vol. 82, no. 5-14, pp. 488–497, Oct. 2007.

[2] N. Mitchell *et al.*, "The ITER magnet system," *IEEE Trans. Appl. Supercond.*, vol. 18, no. 2, Jun. 2008.

[3] H. Bajas *et al.*, "Finite element modelling of cable-in-conduit conductors," *Supercond. Sci. Technol.*, vol. 25, no. 5, Apr. 2012.

[4] R. Riccioli *et al.*, "Mechanical modeling and first case study on ITER TF CICC loading cases with upgraded finite element code simulations," *IEEE Trans. Appl. Supercond.*, vol. 29, no. 5, Aug. 2019, Art. no. 1100110.

[5] R. Riccioli *et al.*, "Advanced modeling of electromagnetic loading of cable-in-conduit conductors for fusion magnets," in *IEEE Trans. Appl. Supercond.*, vol. 30, no. 4, Jun. 2020, Art. no. 4203005.

[6] M. Breschi *et al.*, "Peformance analysis of the toroidal field ITER production conductors," *Supercond. Sci. Technol.*, vol. 30, no. 5, Apr. 2017.

[7] D. Durville, "Numerical simulation of entangled materials mechanical properties," *J. Mater. Sci.*, vol. 40, no. 122, pp. 5941–5948, 2005.

[8] N. Mitchell *et al.*, "The use of Nb_3Sn in fusion: Lessons learned from the ITER production including options for management of performance degradation," *Supercond. Sci. Technol.*, vol. 33, no. 5, Mar. 2020.

[9] H. Bajas, "Numerical simulation of the mechanical behavior of the ITER cable-in-conduit conductors," Ph.D. thesis Ecole Centrale de Paris, Hauts-de-Seine, Châtenay-Malabry, Île-de-France, 2011.

[10] Y. Ilyin *et al.*, "Axial tensile stress-strain characterization of a 36 Nb_3Sn strands cable," *IEEE Trans. Appl. Supercond.*, vol. 16, no. 2, pp. 1249–1252, Jun. 2006.

[11] N. Mitchell, and A. Devred, "2009 ITER magnet design description document 11-7 conductors," ITER Project Internal Document Reference ITER_D_2NBKXY v1.2.

[12] N. Mitchell, "Finite element simulations of elasto-plastic processes in Nb_3Sn strands," *Cryogenics*, vol. 45, no. 7, pp. 501–515, 2005.

[13] M. Breschi *et al.*, "Evaluation of effective strain and $_n$-value of ITER TF conductor samples," *IEEE Trans. Appl. Supercond.*, vol. 21, no. 3, pp. 1969–1973, Jun. 2011.

[14] M. Breschi *et al.*, "Results of the TF conductor performance qualification samples for the ITER project," *Supercond. Sci. Technol.*, vol. 25, no. 9, Jun. 2012.

[15] D. Bessette, "Design of a Nb_3Sn cable-in-conduit-conductor to withstand the 60 000 electromagnetic cycles of the ITER central solenoid," *IEEE Trans. Appl. Supercond.*, vol. 24, no. 3, Jun. 2014, Art. no. 4200505.

[16] M. T. Dylla *et al.*, "Fracture strength distribution of individual Nb_3Sn filaments," *IEEE Trans. Appl. Supercond.*, vol. 26, no. 8, Dec. 2016, Art. no. 6001907.

[17] K. A. Yagotintsev *et al.*, "Overview of the verification tests on AC loss, contact resistance and mechanical properties of ITER conductors with transverse loading up to 30 000 cycles," *Supercond. Sci. Technol.*, vol. 32, no. 10, Sep. 2019.

[18] A. Nijhuis *et al.*, "Change of interstrand contact resistance and coupling loss in various prototype ITER nbti conductors with transverse loading in the twente cryogenic cable press up to 40,000 cycles," *Cryogenics*, vol. 44, no. 5, pp. 319–339, May 2004.

[19] A. Nijhuis *et al.*, "Impact of void fraction on mechanical properites and evolution of coupling loss in ITER Nb_3Sn conductors under cyclic loading," *IEEE Trans. Appl. Supercond.*, vol. 15, no. 2, pp. 1633–1636, Jun. 2005.

[20] M. Chiletti *et al.*, "Void fraction influence on CICCs coupling losses: Analysis of experimental results with MPAS model," *IEEE Trans. Appl. Supercond.*, vol. 30, no. 4, Jun. 2020, Art. no. 4701405.